Influence of the load angle on magnetic radial forces and torque ripple of a low power permanent magnet synchronous machine

Emre Uygun, Michel Hecquet, Abdelmounaïm Tounzi, Daniel Depernet, Vincent Lanfranchi, Serge Bruno, Thierry Tollance

Version of Record: https://www.sciencedirect.com/science/article/pii/S0378475420301798
Manuscript_50c8e2acadabd8e09181a59d9b2b89bd

Influence of the load angle on magnetic radial forces and torque ripple of a low power permanent magnet synchronous machine

Emre Uygun[1,4], Michel Hecquet[1], Abdelmounaïm Tounzi[1], Daniel Depernet[2], Vincent Lanfranchi[3], Serge Bruno[4], Thierry Tollance[1,4]

[1]Univ. Lille, Arts et Metiers ParisTech, Centrale Lille, HEI, EA 2697 - L2EP - Laboratoire d'Electrotechnique et d'Electronique de Puissance F-59000 Lille, France
Bâtiment ESPRIT, Cité Scientifique, 59650 Villeneuve-d'Ascq, France, emre.uygun@centralelille.fr, michel.hecquet@centralelille.fr
[2]FEMTO-ST, CNRS Univ. Bourgogne Franche-Compte
Belfort, France
[3]CNRS FRE 2012 Roberval, Centre de recherche Royallieu, CS 60 319, Sorbonnes Universités, Universtié de Technologie de Compiègne Compiègne Cedex, France
[4]SOMFY ACTIVITES SA, 50 avenue du Nouveau Monde, 74300 Cluses, France

ARTICLE INFO

Article history:
Received 15 October 2019
Received in revised form 14 Jan. 2020
Accepted 00 February 00

Keywords:
Radial magnetic force
Torque ripple
Control
Load angle
Permanent magnet machine

ABSTRACT

This paper shows the influence of the shift phase angle ψ between phase currents and back-electromotive forces on magnetic radial forces and torque ripple for a specific low power permanent magnet synchronous machine. This influence is firstly demonstrated through analytical development considering only the first harmonic values. Then, magnetic pressure harmonics versus space and frequency as well as torque ripple are evaluated on the studied motor for different angles using finite element approach. The aim is to establish a good compromise between consumed current, torque and radial force harmonics at the origin of the electromagnetic noise. Experimental measurements with a sensorless field-oriented control are detailed.

1. Introduction

Nowadays, electric machines dedicated to the automotive and domestic applications are increasingly subject to severe acoustic requirements including restrictive noise level standards. These applications use generally low power motors of 20 W classically supplied by AC 230V RMS network or DC supply (12 - 24V).

The acoustic emission of electric machines is due to several causes including the electromagnetic forces acting on the stator armature. The acoustic behaviour can basically be improved by modifying the machine structure to reduce the radial component of magnetic origin force [1, 2] or to move the stator natural frequencies away from those of the exciting forces [3]. A recent mean of passive reduction of magnetic forces is done by connecting capacitors to the stator damper windings [4]. However, the proposed solutions cannot always be suitable with manufacturing process requirements, and generally, a compromise must be taken to reduce the radial forces without compromising the torque, which relies on multi-objective optimization processes [5].

Another way to reduce the noise caused by magnetic forces can be achieved by adapting the control algorithms. These methods, qualified as active, have the advantage of being independent of the machine design. Many techniques have been studied in the last decades, such as random switching techniques for PWM-controlled induction drives [6], which aimed at reducing the high-frequency borne tone, but without changing the total sound pressure level. Controlling currents to reduce the emitted noise has also been studied by many authors [7, 8]. It is mainly carried out by choosing the appropriate non sinusoidal waveforms of the supply currents, i.e. by injecting specific harmonics, but this requires an accurate system to control high frequency current harmonics. Finally, methods based on smoothing directly the magnetic forces have been studied [9] for switched reluctance synchronous machines, as well as semi active methods relying on the control of piezoelectric actuators [10], or by injecting current harmonics in an auxiliary winding [11].

In the particular case of permanent magnet synchronous machines (PMSM) with surface mounted permanent magnets, two control parameters given by the average torque relation at steady state (2), i.e. the current phase magnitude and the load angle, can be used to potentially mitigate the electromagnetic noise. Some authors have studied this possibility [12-14]: they mainly conclude that the influence of the load angle is not the same on each magnetic pressure harmonic as it depends on the machine structure. Therefore, no rules concerning the setting of this parameter to reduce the noise or experimental measurements are available. Besides, as the load angle has a direct influence on the average torque (2), a compromise must be found to reach the optimal load angle that mitigates the noise while keeping the average torque value as high as possible.

This paper deals with the study of the influence of the load angle on the magnetic pressure harmonics, including the noise, in constant torque configuration, on a low power machine, which is uncommon. Firstly, an analytical approach is presented to demonstrate the influence of the load angle on the radial pressure. Then, 2D Finite Element Modelling (FEM) simulations are conducted with different load angles, at the same average torque, to determine variation laws of radial force and torque harmonics. Finally, experimental measurements are relied on to validate the presented approach.

2. Analytical approach

2.1. Definitions and torque expression

In the case of a sinusoidal machine, its electrical values can be represented by rotating vectors, using the following fundamental equation:

$$\bar{V} = R_s \cdot \bar{I_s} + jX_s\bar{I_s} + \bar{E} \qquad (1)$$

where V represents the phase voltage, I_s the phase current, E the back-electromotive force (back-EMF), R_s and X_s the stator armature resistance and reactance respectively. The load angle ψ is defined as the electric angle from the current vector to the back-EMF vector (Fig. 1).

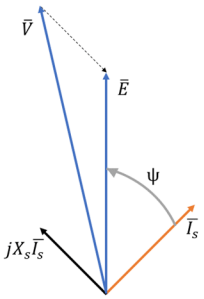

Fig. 1 - Synchronous machine phasor diagram (with a negligible value of R_s).

Therefore, the expression of the average electromagnetic torque is given by the well-known classical expression (2).

$$T_{avg} = 3\bar{E} \cdot \bar{I_s}/\Omega = 3 \cdot p \cdot I \cdot \Phi \cdot \cos(\psi) \qquad (2)$$

where p is the pole pair number, I the RMS value of the phase current, Φ the RMS value of the rotor magnetic flux. This relation shows that the load angle has a direct effect on the average torque.

Generally, phase currents and corresponding back-EMFs are usually set in phase to produce the maximal torque per ampere in order to improve the efficiency ($\psi = 0$). However, some operating points may need flux weakening to reach high speeds. This is done by shifting the phase currents with respects to the back-EMFs, resulting in a negative load angle ($\psi < 0$).

2.2. Radial magnetic pressure expression development

Relation (2) clearly shows the influence of the load angle on the average torque. Its influence on the radial pressure is demonstrated analytically in the following.

The radial magnetic flux density in the air gap can be calculated based on the well-known permeance-magnetomotive force approach (3).

$$B_{rad} = \Lambda_g \cdot (MMF_s + MMF_r) \qquad (3)$$

where MMF_s and MMF_r are the stator and rotor magnetomotive forces respectively, and Λ_g the magnetic permeance of the airgap (per surface unit).

Under the assumption of sinusoidal quantities,

- the stator excitation of phase q is written as:

$$I_{sq}(t) = I\sqrt{2}\, sin(\omega_s t - (q-1) \cdot 2\pi/3 - \psi) \qquad (4)$$

where ω_s is the electric angular velocity.

- and the winding function of the phase q by the relation:

$$W_{fq}(\theta) = W \cos(p\theta - (q-1) \cdot 2\pi/3) \qquad (5)$$

where W is its amplitude which can be obtained from a fast Fourier transform (FFT) of the real winding function and θ the angle.

The stator magnetomotive force can then be determined such as:

$$\begin{aligned} MMF_s(t,\theta) &= \sum_{q=1}^{3} I_{sq} W_{fq} \\ &= 3\mathrm{WI}/2 \cdot \sin(\omega_s t - p\theta - \psi) \\ &= A \sin(\omega_s t - p\theta - \psi) \end{aligned} \qquad (6)$$

In a similar manner, the rotor magnetomotive force due to the magnets can be expressed as follows:

$$MMF_r(t,\theta) = B_r l_m/\mu_0\mu_{rm} \cdot \sin(\omega_s t - p\theta - \pi/2)$$
$$= B\sin(\omega_s t - p\theta - \pi/2) \quad (7)$$

where B_r is the remanent flux density, l_m the thickness of the magnet, μ_{rm} its relative permeability and μ_0 the vacuum magnetic permeability. The MMF_r is shift phased by 90° with respect to the MMF_s so that the maximal torque is obtained for $\psi = 0$.

In the case of parallel magnetized magnets, the MMF can effectively be considered having a pure sinusoidal waveform.

With a smooth rotor, the airgap permeance is considered as a constant equal to the mean value Λ_0, corrected with the Carter coefficient to account for stator slot effects.

With these hypotheses, the radial magnetic flux density can take the following expression:

$$B_{rad}(t,\theta) = \Lambda_0\sqrt{A^2 + B^2 + 2AB\sin(\psi)}\cos(\omega_s t - p\theta + \varphi) \quad (8)$$

with

$$\varphi = \tan^{-1}(A\cos(\psi)/(B + A\sin(\psi))) \quad (9)$$

In this simplified case, the radial component contains only a fundamental waveform, whose amplitude varies with respect to the load angle (Fig. 2).

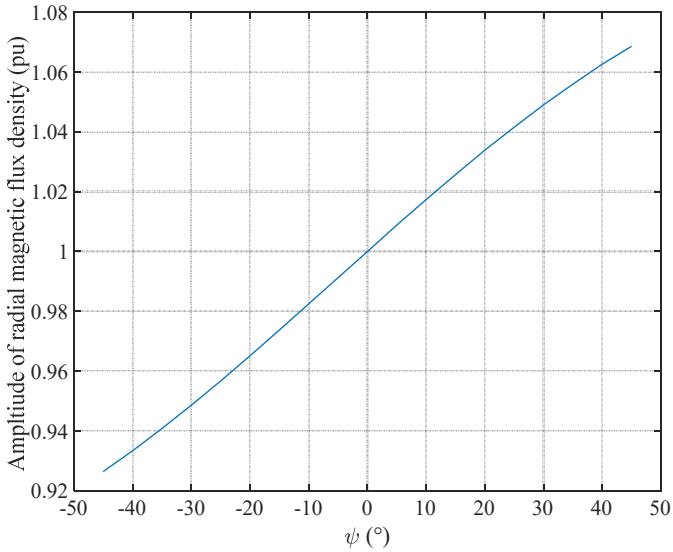

Fig. 2 - Radial flux density amplitude versus load angle.

Neglecting the contribution of the tangential component of the magnetic flux density, the radial pressure can then be determined analytically using Maxwell stress tensor:

$$\sigma_{rad} \approx {B_{rad}}^2/2\mu_0 \quad (10)$$

leading to the following expression:

$$\sigma_{rad} = \sigma_0(\psi) + \sigma_{(-2p,2)}(\psi) \cdot \cos(2\omega_s t - 2p\theta + 2\varphi) \quad (11)$$

with

$$\sigma_0 = \sigma_{(-2p,2)} = {\Lambda_0}^2/4\mu_0 \cdot (A^2 + B^2 + 2AB\sin(\psi)) \quad (12)$$

The radial pressure is constituted of two harmonics, the mean value and a harmonic at $(-2p, 2)$ resulting from the interaction between the first harmonics of the magnetomotive forces. The obtained orders are twice the magnetomotive force ones: $(-2p, 2) = 2 \times (-p, 1)$. These two harmonics have the same amplitude and are function of the load angle too (Fig. 3).

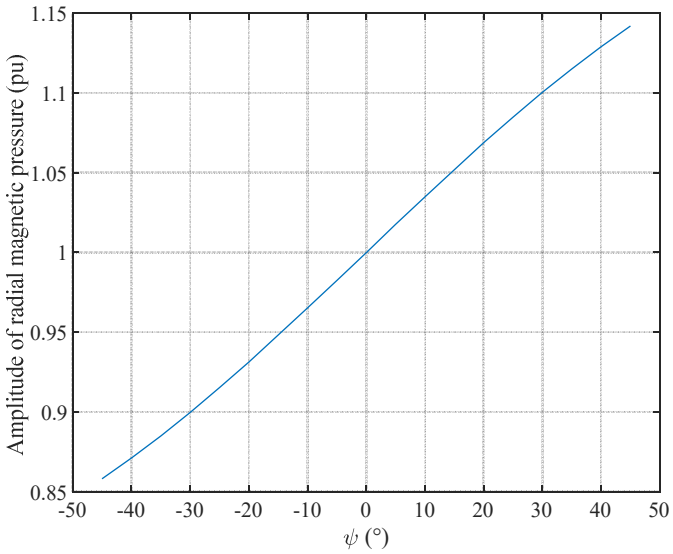

Fig. 3 - Variation of the radial magnetic pressure amplitude against the load angle.

Finally, the influence of the load angle on the magnetic radial pressure harmonics can easily be demonstrated in case of pure sinusoidal waveform of the different variables. Taking into consideration the expression of the average torque (2), it can be concluded that there will be a compromise to reach in order to maintain the maximum torque per ampere while increasing or decreasing this radial force harmonic.

In the case of a real machine, it can be showed that each pressure harmonic is function of the load angle. This will not be demonstrated analytically, but through finite element computation.

3. FEA simulation methodology

The studied machine is a 230 V, 3000 rpm three phase surface mounted PMSM prototype at design stage with 6 stator slots (Z_s) and 4 poles ($p = 2$).

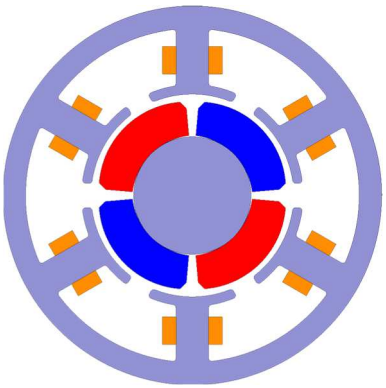

Fig. 4 - Cross section of the studied machine.

The phase conductors are wound around each tooth (Fig. 4) leading to a fractional slot concentrated winding (FSCW) type machine, thus reducing the production costs.

The main characteristics of the studied machine are summarized in Table 1.

Table 1 - Main characteristics.

Winding type	Concentrated winding
Stator length	15 mm
Stator external diameter	< 50 mm
Lamination thickness	0.65 mm stator / solid rotor
Power	20 W
Air gap	0.4 mm
Magnet type	Ferrite
Magnet volume	1932.10e^{-6} m^3
Remanent flux density (B_r)	0.4 T
Pole pairs (p)	2
Number of slots (Z_s)	6

3.1. Simulation process

To quantify the effect of the load angle on each radial pressure harmonic, simulations were carried out using 2D FEM model (ANSYS Maxwell software). Calculations were achieved at rated speed, considering the nonlinear behaviour of the magnetic material while the armature windings were supplied by purely sinusoidal phase currents, whose magnitude are function of the load angle. A view of the modelled domain mesh (17,424 elements) is shown in Fig. 5a. Besides, the simulation time step used is of 24.2 microseconds.

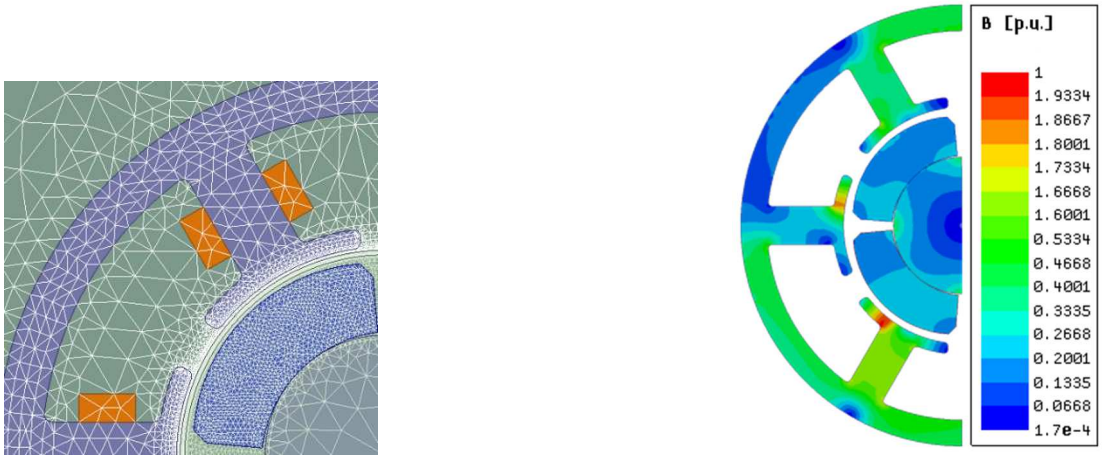

(a) (b)

Fig. 5 - (a) Mesh view; (b) Magnetic induction field map.

Thus, simulations were conducted by varying the load angle by 10° step and applying phase currents whose magnitudes are determined using relation (13) bellow (Fig. 6a), so that the average torque remains at the same value for all angles (Fig. 6b). To avoid high magnitude currents, their increase rate has been limited to 15%, thus limiting the range of the load angle between -30° and +30°.

$$I_\psi = I_r/\cos(\psi) \qquad (13)$$

where I_r is the RMS rated phase current, giving the rated torque at $\psi = 0$.

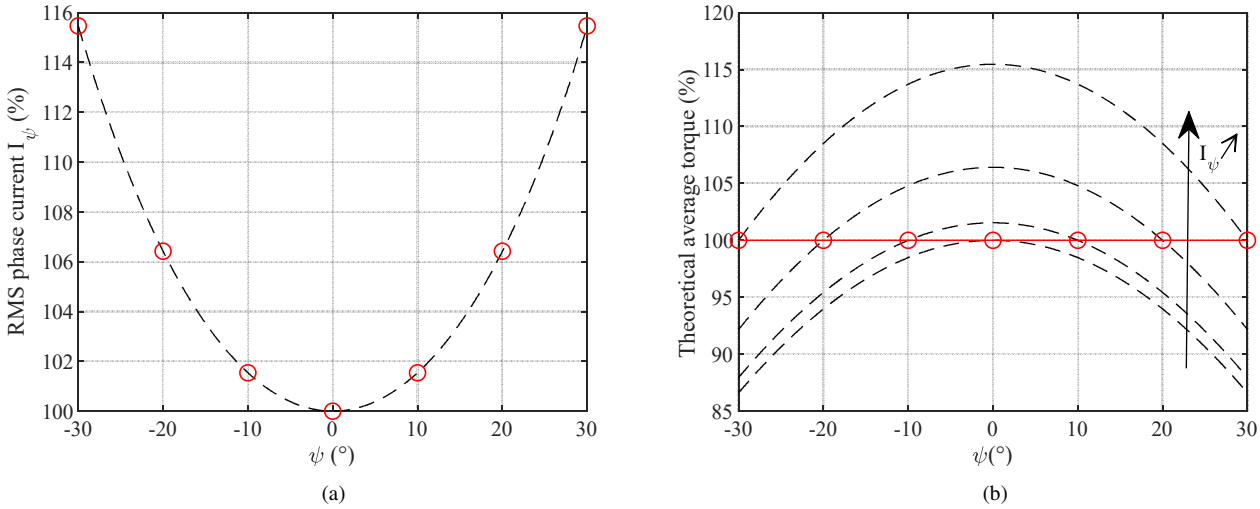

Fig. 6 - (a) Ratio of applied RMS phase currents on the RMS rated current (red circles); (b) ratio of theoretical average torque on the rated torque [theoretical average torque versus ψ for a given phase current I_ψ (dashed), theoretical average torque obtained for each load angle (circles)]; versus the load angle.

3.2. Simulation process

The obtained values of the magnetic flux density in the airgap (radial B_{rad} and tangential B_{tan}) versus time and space are then used to calculate the radial magnetic pressure in the airgap (14).

$$\sigma_{rad}(t,\theta) = (B_{rad}(t,\theta)^2 + B_{tan}(t,\theta)^2)/2\mu_0 \qquad (14)$$

As the emitted noise is mainly due to the spatial and temporal harmonics of the radial pressure [1,2], the latter are computed using a 2D FFT (15).

$$\sigma_{rad}(t,\theta) = \sum_{m,n} \sigma_{mn} \exp(j(2\pi n f_s t - m\theta + \varphi_\sigma)) \qquad (15)$$

where m represents the number of wave or spatial order, n the temporal order, σ_{mn} the amplitude of pressure harmonic and φ_σ the shift phase.

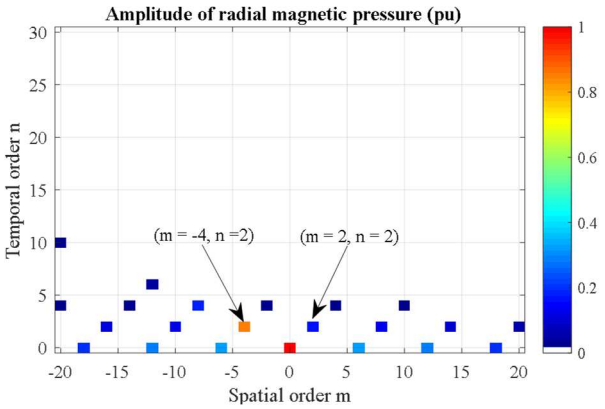

Fig. 7 - 2D FFT of radial magnetic pressure for ψ = 0 (ratio on the mean value).

As expected, in Fig. 7, the spatial and temporal harmonic content is quite rich which is particular to FSCW type PMSMs [16, 17]. The harmonic $(-4, 2)$ of radial pressure has the highest magnitude as it is linked to the amplitude of each fundamental waveform (see section 2.2). The $(2, 2)$ is typical for the FSCW type machines, verified by the Greatest Common Divider (GCD) between the number of stator teeth and the number of poles $(Z_s, 2p)$ [15, 16]. Although they are not visible in Fig. 7, there are a lot of harmonics until the 30th temporal order and beyond, but their amplitude is very low.

Following the same reasoning done to reach equation (12), harmonic consideration can lead to understand the origin of the pressure harmonics. Indeed, in the real machine, the winding function and the airgap permeance (due to stator slots) are constituted of several spatial harmonics, which induce spatial harmonics in the radial pressure spectrum, spaced by Z_s. Regarding the temporal harmonics, in the case of sinusoidal currents, they are induced only by

the small saliencies of the rotor and the harmonics of the rotor magnetomotive force. As a result, pressure harmonics are spaced by p in the temporal axis, as there are p rotor poles in one electrical period (or $1/p$ mechanical revolution).

Within the scope of acoustic noise reduction study, as the generated noise is inversely proportional to the spatial order $(1/m^4)$, focus will be devoted to low spatial orders of pressure [1,2], which are 0, 2 and 4. Their amplitudes are given in the following Table 2.

Table 2 - Amplitudes of low spatial orders of radial pressure harmonics for ψ = 0 (ratio on the mean value).

(m,n)	(-4,2)	(2,2)	(4,4)	(-2,4)	(0,6)
Amplitude (pu)	0.8537	0.168	0.0221	0.0178	0.0061
(m,n)	(-4,8)	(2,8)	(4,10)	(-2,10)	(0,12)
Amplitude (pu)	0.0033	0.0021	0.002	0.0019	0.0016

The frequencies of these main harmonics are multiple of $2f_s$ (2, 4, 6, 8, 10,…) and some of them ($2f_s$, 8fs, $20f_s$, $22f_s$) are the highest ones noticeable in vibration and acoustic measurements (arrows in Fig. 8).

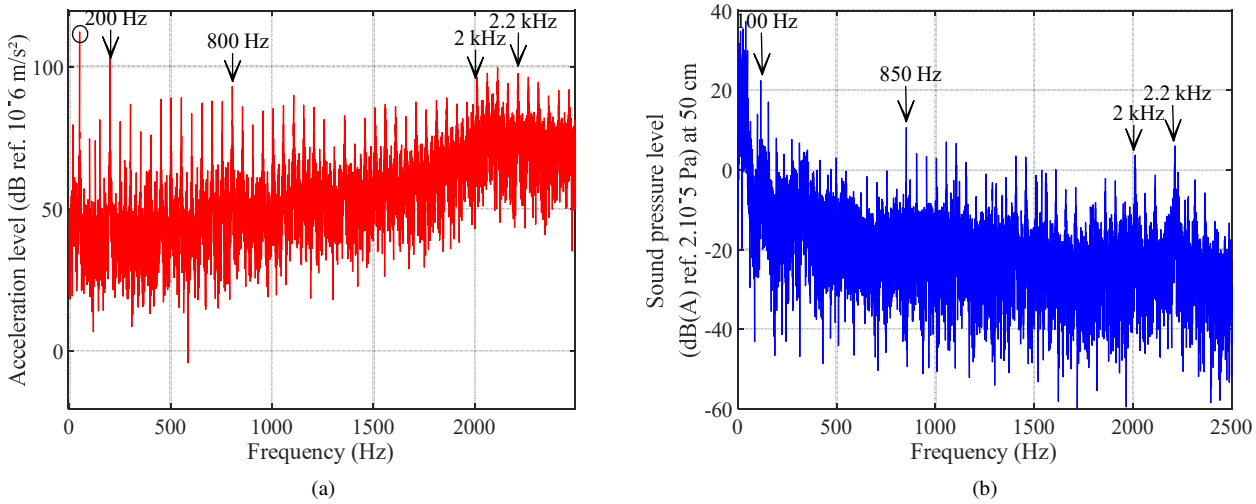

Fig. 8 - Experimental measurements under no-load conditions (a) Acceleration spectrum; (b) Sound pressure spectrum.

A lot of harmonics, multiple of 50 Hz, are also visible between these main harmonics. This is due to the rotor eccentricities shown by the higher acceleration harmonic at 50 Hz (circle in Fig. 8a). Accordingly, main sound pressure harmonics may be shifted by multiple of 50 Hz (e.g. arrows at 100 Hz and 850 Hz in Fig. 8b). This phenomenon was not considered in the simulation process. So, it is already known that these imperfections on the real machine will complicate the validation of the simulation results, since each measured vibration and noise harmonic may be modified due to this eccentricity. However, a look at the global tendencies can validate our approach.

Besides, the highest harmonics of sound pressure level spectrum at low frequencies (harmonics under 40 Hz in Fig. 8b) are due to the background noise (identified as the noise generated by the fan of the AC supply). As they are not due to the motor itself, it should not be considered for this study.

The resonance frequencies associated to each mode-shape of this machine are given by finite element calculation [17], and were verified through measurements. As the 2nd mode-shape has the lowest resonance frequency (2.2 kHz) the amplitude of the associated transfer function is much higher than others at low frequencies (Fig. 9). Moreover, knowing that magnetic force harmonics are rather high at low frequencies, the excitation of the modes-shape 2 by the radial force harmonics of spatial order 2 will result in a high amount of displacement. That is why focus on reducing the radial pressure harmonics of this 2nd mode-shape will be done. In the case of the mode-shape '0', the breathing mode [18], the resonance frequency is very high (13 kHz), so its impact on the noise is negligible.

Regarding the pressure harmonics of the same spatial order which are close the resonance frequency of the 2nd mode-shape ($\sigma_{(2,20)}$ and $\sigma_{(-2,22)}$), their amplitude is very low (0.0001 pu). However, as the amplitude of the transfer function is maximal within the range of [2000;2200] Hz, resulting acceleration and acoustic harmonics are noticeable at these frequencies. Thus, these high frequency harmonics will be considered as well.

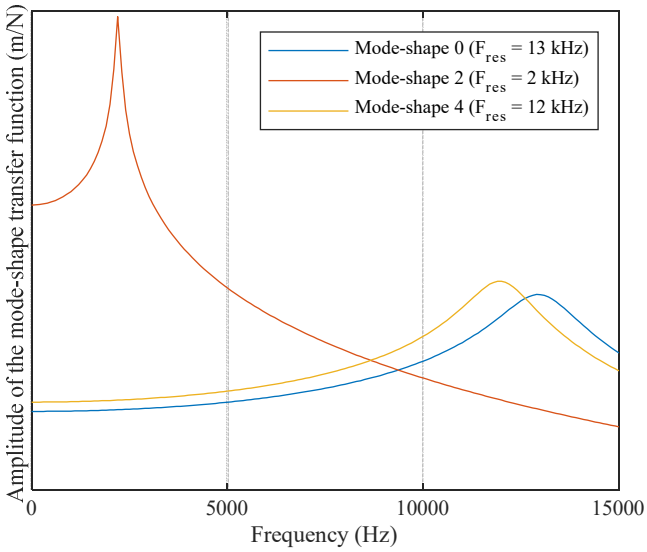

Fig. 9 - Low order mode shapes (illustration by analytical expressions corrected with measured natural frequencies).

4. Simulation results

4.1. Average torque and torque ripple

The average torque obtained from FEA is not constant within the range of load angle values. For simulations at rated torque, a variation of 3% can be observed between torques at the extreme values of the load angle (Fig. 10a). This is due to the assumption of pure sinusoidal back EMF waveform made during the calculation of RMS phase current for each load angle, which is not exactly the case, due to the spatial harmonics of the rotor magnetomotive force.

Torque ripple has been calculated using the classical relation (16) and its variation with respect to ψ seems to be linear (Fig. 10b).

$$T_{ripple} = (T_{max} - T_{min})/T_{avg} \qquad (16)$$

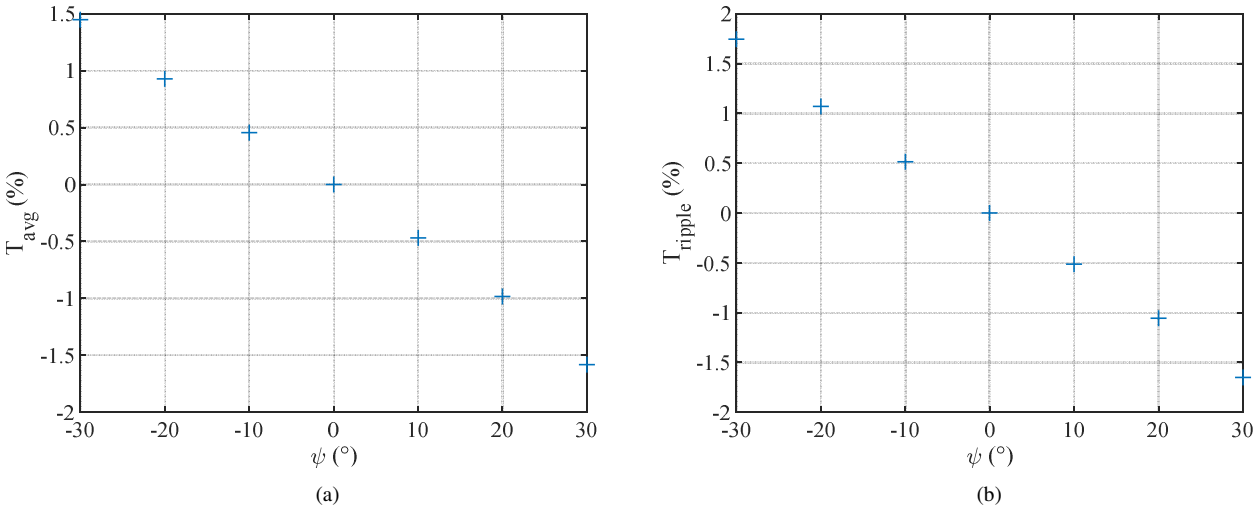

Fig. 10 - Waveform of (a) average torque (ratio on the optimal torque $T_{avg}(\psi = 0)$); (b) torque ripple; versus the load angle.

4.2. Radial magnetic pressure harmonics

Following the approach detailed in section 3.2, the variation of each radial force harmonic versus ψ can be observed, especially, the highest pressure harmonics (circles in Fig. 11) and the pressure harmonics nearest to the resonance (crosses in Fig. 11) of the spatial order 2. The amplitudes have been divided by $\sigma_{mn}(\psi = 0)$.

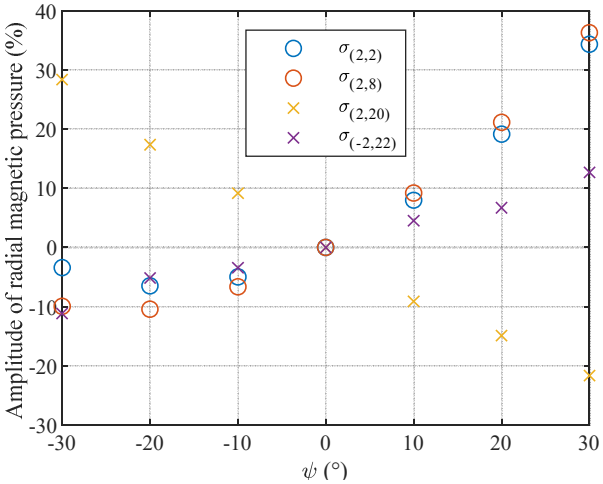

Fig. 11 - Variation of main radial pressure harmonics versus the load angle ((2,2) in blue circles, (2,8) in red circles, (2,20) in yellow crosses, (-2,22) in purples crosses).

With these laws, it is possible to determine the control strategy, i.e. the optimal load angle which gives a good compromise between the different constraints; radial pressure of a specific spatial and time order, torque ripple, or efficiency. This will depend on the weight given to each constraint.

4.3. Average torque and torque ripple

A comparison between different strategies has been chosen: an operation at the optimal torque per ampere (MTPA) which is the usual control strategy (ψ = 0°), and operation at field weakening (FW) with -20° phase shift, which reduces significantly the low-frequency radial pressure harmonics of spatial order 2. However, the latter increases significantly the consumed current and the torque ripple. Therefore, a comparison with a -10° field weakening strategy which gives a good compromise between the different variables is also added in the following Table 3.

Table 3 - Comparison between two FW strategies (ψ = -10°/-20°) with respect to the MTPA strategy (ψ = 0°).

ψ	-10°	-20°
Average torque	+ 0.46%	+ 0.93%
Torque ripple	+ 0.51 %	+ 1.1 %
RMS phase current	+ 1.8 %	+ 6.5 %
Stator copper loss	+ 3.3 %	+ 13 %
$\sigma_{(2,2)}$	- 5 %	- 6.5 %
$\sigma_{(2,8)}$	- 6.7 %	- 10 %

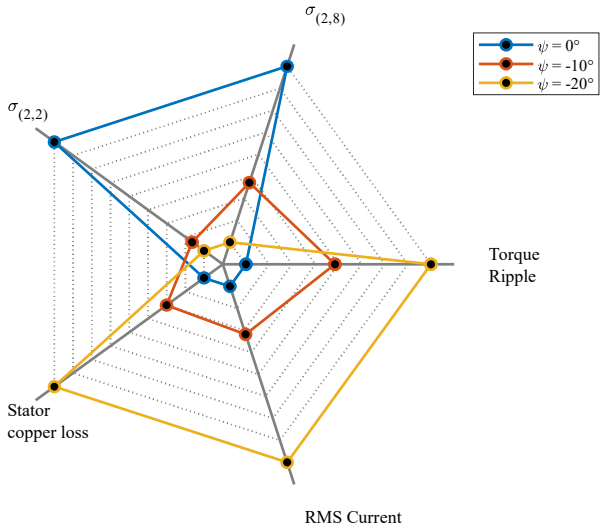

Fig. 12 - Comparison of the performances for different load angles.

The radar plot of Fig. 12 shows that field weakening strategy at -10° gives a good compromise to reduce the radial forces of spatial order 2 while limiting the increase of current and torque ripple.

Since the studied motor is designed for an application that needs only low noise operation without any care about torque ripple, field weakening strategy at -20° gives the best results for this purpose. However, in this case the efficiency decreases significantly because of an increase on the phase current.

5. Experimental measurements

Acceleration and acoustic pressure measurements were conducted in a semi-anechoic room. The motor was at no load to avoid the influence of the test bench and the load. A sensorless field-oriented control (FOC) was used to achieve experimental measurements while varying the d-axis current to achieve field-weakening (or field-boosting) and keeping the q-axis current constant to maintain the same torque.

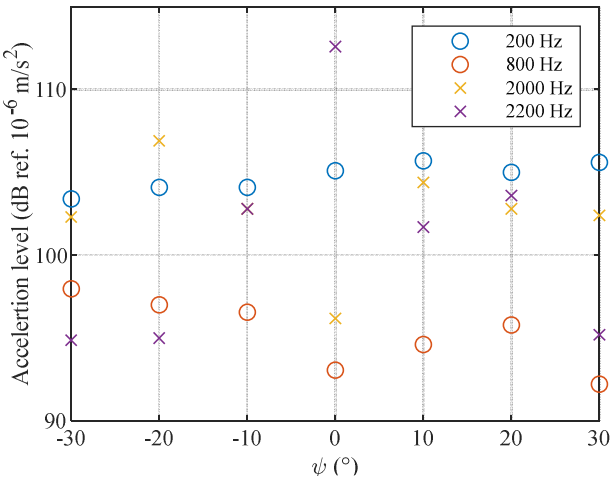

Fig. 13 - Acceleration level versus the load angle at given frequencies [200 Hz (blue), 800 Hz (orange), 2000 Hz (yellow), 2200 Hz (purple)], obtained from experimental measurements at no-load operation.

As shown in Fig. 13, all acceleration harmonics do not have the same variation as calculated radial pressure harmonics. Only the harmonic at 200 Hz varies as the magnetic pressure harmonic $\sigma_{(2,2)}$. Regarding the high frequency acceleration harmonics at 2000 and 2200 Hz, their variation is not monotonic. These local variations may be due to measurement errors. As for the acceleration harmonic at 800 Hz, its variations are opposed to the ones of the pressure harmonic $\sigma_{(2,8)}$. These non-monotonic and inverse variations can be explained by the rotor eccentricities, which increase and decrease some harmonics, as explained in section 3.2.

Fig. 14 shows the variation of the total sound pressure level versus the load angle. Measurements at no load condition make us conclude that, under sinusoidal supply at no load, varying the load angle does not have a real impact on the noise level, if the tendency is observed. This can be explained by the rather low level of pressure harmonics, which do not excite enough the natural frequencies of the stator under sinusoidal supply. Accordingly, the influence of the load angle on pressure harmonics is also low: a maximum reduction of 10% is noticeable in Fig. 11 and Table 3. Another explanation could be the opposite variation of different pressure harmonics, keeping the total sound pressure at the same level.

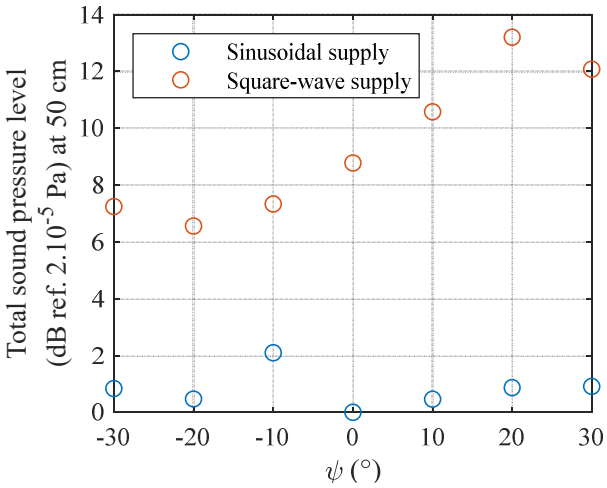

Fig. 14 - Total sound pressure level (A-weighted, scaled to 0 dB for ψ = 0 with a sinusoidal supply) versus the load angle for two different current waveforms [sinusoidal (blue), square wave (red)], obtained from experimental measurements at no-load operation.

As a comparison, measurements were also carried out using a square-wave current supply used to control brushless DC machines. With this type of supply, the influence of the load angle on the noise becomes significant (2 dB reduction between 0° and -20°), since harmonics of the supply current are high enough to excite the machine resonance frequencies.

6. Conclusions

This study shows that radial magnetic pressure harmonics are function of the load angle. This result has been demonstrated analytically in the simplified case under the assumption of pure sinusoidal variables of the machine. 2D FEM simulations allowed us to confirm this statement, and give, for different load angles and almost the same average torque, the variation laws of radial pressure and torque harmonics. These results show that flux weakening strategy can reduce radial magnetic pressure harmonics, like almost all harmonics of spatial order 2. Experimental measurements on an uncommon low power PMSM in the case of a sinusoidal supply with a sensorless field-oriented control allowed us to validate these simulation results only for the main radial pressure harmonic, due to the motor imperfections. Besides, under sinusoidal supply, the machine is not excited enough, making the influence of the load angle on noise negligible. However, with a square-wave supply, which can be favoured for cost purposes, the influence of the load angle on the noise becomes significant, making this mean of noise reduction more interesting.

REFERENCES

[1]. Jacek F. Gieras, Chong Wang, Joseph Cho Lai, Noise of Polyphase Electric Motors – 1st Edition, CRC Press, 2005.

[2]. S. J. Yang, *Low-Noise Electrical Motors*, Oxford, 1981.

[3]. Jung-Pyo Hong, Kyung-Ho Ha, Ju Lee, "Stator pole and yoke design for vibration reduction of switched reluctance motor", IEEE Transactions on Magnetics, Vol. 38, No. 2, March 2002.

[4]. Grégory Bauw, François Balavoine, Bertrand Cassoret, Olivier Ninet, Raphaël Romary, "Equivalent circuit of PWM-fed induction machine with damper winding for noise and vibration reduction", IEEE Transactions on Industry Applications, Vol. 54, No. 5, September-October 2018.

[5]. Zuo Shuguang, Hu Xiaorui, Zhang Yaodan, Wu Shuanglong, "Rotor shape optimization of claw-pole alternator to reduce acoustic noise caused by electromagnetic forces", IEEE Transactions on Energy Conversion, Vol. 34, No. 4, Dec. 2019.

[6]. Thomas G. Habetler, Deepak Divan, "Acoustic noise reduction in sinusoidal PWM drives using a randomly modulated carrier", IEEE Transactions on Power Electronics, Vol. 6, No. 3, July 1991.

[7]. Weidong Zhu, Babak Fahimi, Steve Pekarek, “A field reconstruction method for optimal excitation of permanent magnet synchronous machines”, IEEE Transactions on Energy Conversion, Vol. 21, No. 2, June 2006.

[8]. Pierre Pellerey, Gwennael Favennec, Vincent Lanfranchi, Guy Friedrich, “Active reduction of electrical machines magnetic noise by the control of low frequency current harmonics”, IECON 2012 - 38th Annual Conference on IEEE Industrial Electronics Society, Montreal, QC, Canada, 25-28 Oct. 2012.

[9]. Andreas Hofmann, Ahmed Al-Dajani, Matthias Bösing, Rik W. De Doncker, “Direct instantaneous force control: A method to eliminate mode-0-borne noise in switched reluctance machines”, 2013 International Electric Machines & Drives Conference, Chicago, IL, USA, 12-15 May 2013.

[10]. Xavier Mininger, Elie Lefeuvre, Mohamed Gabsi, Claude Richard, Daniel Guyomar, “Semiactive and Active Piezoelectric Vibration Controls for Switched Reluctance Machine”, IEEE Transactions on Enecrgy Conversion, Vol. 23, No. 1, March 2008.

[11]. Jean-Philippe Lecointe, Raphaël Romary, Jean-François Brudny, Mike McClelland, “Analysis and active reduction vibration and acoustic noise in the switched reluctance motor”, IEE Proceedings - Electric Power Applications, Vol. 151, No. 6, pp. 725-733, November 2004.

[12]. Pierre Pellerey, Vincent Lanfranchi, Guy Friedrich, “Influence of the load angle on the magnetic pressure harmonic content of a WRSM”, IECON 2010 - 36th Annual Conference on IEEE Industrial Electronics Society, Glendale, AZ, USA, 7-10 Nov. 2010.

[13]. Sebastian Rick, David Franck, Kay Hameyer, “Hybrid NVH Simulation for Electrical Vehicles I - Force Excitation Model for Electrical Machines”, DAGA 2015, Nürnberg, March 2015.

[14]. Jean Le Besnerais, Emile Devillers, Michel Hecquet, Jean-Philippe Lecointe, “Effet de l’angle de charge sur les harmoniques d’efforts magnétiques dans les machines synchrones à aimants permanents en surface”, Symposium de Génie Electrique, Grenoble, France, June 2016.

[15]. Jean Le Besnerais, “Vibroacoustic Analysis of Radial and Tangential Air-Gap Magnetic Forces in Permanent Magnet Synchronous Machines” IEEE Trans On Magnetics, Vol. 51, No. 6, June 2015.

[16]. Patricio La Delfa, F. Gillon, M. Hecquet, “Analysis of radial force harmonics in PMSM responsible for electromagnetic noise: contribution of the lowest harmonics”, IEEE Trans On Magnetic, Vol. 52, No. 11, November 2016.

[17]. Thierry Tollance, Michel Hecquet, Frédéric Gillon, Abdelmounaïm Tounzi, “Design of low power motors with a good compromise between ripple torque and radial forces”, 2018 XIII International Conference on Electrical Machines (ICEM), Alexandroupouli, Greece, 3-6 Sept. 2018.

[18]. A. Hofmann, F. Qi, T. Lange, R. W. De Doncker, “The breathing mode-shape 0: Is it the main acoustic issue in the PMSMs of today’s electric vehicles?”, 17th International Conference on Electrical Machines and Systems (ICEMS), Hangzhou, China, 22-25 Oct. 2014.